FOI-R--0167--SE
October 2001
ISSN 1650-1942
User report

Mattias Unosson

Modelling of concrete material behaviour with application to reinforced concrete beams subjected to impact

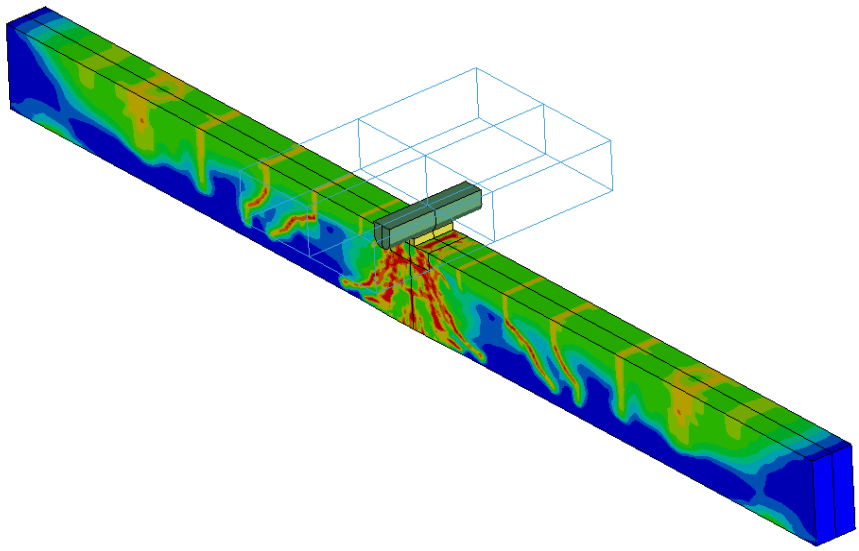

Weapons and Protection
SE-147 25 Tumba

SWEDISH DEFENCE RESEARCH AGENCY

Weapons and Protection
SE-147 25 Tumba

FOI-R--0167--SE

October 2001

ISSN 1650-1942

User report

Mattias Unosson

Modelling of concrete material behaviour with application to reinforced concrete beams subjected to impact

Table of contents

1 INTRODUCTION

The Swedish Armed Forces Headquarters (HKV) finances the project "Structural protection for stationary and mobile tactical behaviour" at the Swedish Defence Research Agency (FOI). The overall goal for this project is to develop methods and techniques for modelling of weapons effects in order to provide a basis for the development of structural protection for stationary and mobile tactical behaviour. The research is therefore carried out with the purpose to develop knowledge concerning protection in new environments and through theoretical and experimental research develop and verify methods of evaluation and optimization of the protection ability of objects by using different simulation models of weapons effects, material behaviour and structural response.

Within the framework of this project well monitored drop weight tests were performed 1999 at FOI in order to get a sound basis for verification of tools for numerical simulations. In 2001 these tests were simulated numerically using the commercial finite element code LS-DYNA together with a mechanical constitutive model for concrete called K&C Concrete model. The purpose of this study was to evaluate the ability of the chosen numerical method and material models to predict the material and structural response. This work is presented here.

2 TESTS

In the tests performed at FOI in 1999, reinforced concrete beams were subjected to impact loading using a drop weight (see Figure 2-1). The beams were 4.2 m and simply supported 0.1 m from the ends with a 0.17x0.34 m cross-section. The reinforcement consisted of four ø12 mm rebars and 22ø10 mm stirrups. The drop weight had a mass of 718 kg and the cylindrical striker head impacted a steel pad fixed to the beam at 6.7 m/s. Dampers were used to stop the drop-weight after 90 mm of vertical displacement of the beam, corresponding to approximately 20 ms after impact. Four beams were tested during which the following registrations were made:

1. Displacement history from high speed photos of the beam mid-section (Photo)
2. Striker displacement history (TranS)
3. Striker head acceleration history (AccS)
4. Indication of contact between striker head and impact pad (Contact)
5. Beam acceleration history 100mm to the left and right respectively of the point of impact (AccL and AccR)
6. Beam displacement history at mid-section (TranB)
7. Crack indication at beam side 20 mm above lower surface of beam (Crack)
8. Strain history in lower rebars 200 mm from mid-span (SGR-side)
9. Strain history in lower rebars at mid-span (SGR-mid)
10. Strain history at the concrete surface at mid-span and at the same height as rebars (SGC)

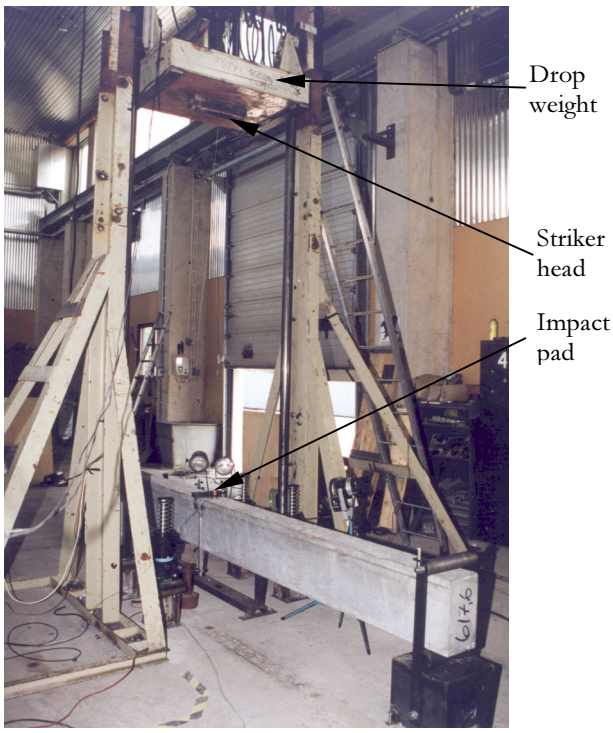

Figure 2-1 Drop weight test set-up.

Not all the registrations were successful which is evident in the figures of comparison in chapter 6. The test set-up and results are thoroughly presented in [1].

3 MECHANICAL MATERIAL CHARACTERIZATION

The concrete material and steel material for the reinforcement were characterized to obtain data for the numerical analysis. No mechanical characterization of the drop weight materials, concrete and steel, was performed.

3.1 Concrete material

Optiroc produced the concrete with the mix proportions, according to the supplier's specifications, in Table 3-1.

Table 3-1 Concrete mix proportions

Cement	440 kg m^{-3}
Ballast	Porphyric granite, 0-20 mm
Water	145 kg m^{-3}
Additives	Not specified

The used concrete type was mechanically characterized at several occasions through weighing of test specimens, uniaxial compression of 150x150 mm cubes and ø100x200 mm cylinders and split tensile tests on 150x150 mm cubes. The fracture energy release was determined from RILEM beam testing [2]. Confined uniaxial compression of ø75x150 mm cylinders was performed by the Norwegian Defence Research Establishment (FFI) with the gauged reactive confinement (GREAC) cell, see [3]. The initial mass density was 2420 kg/m^3. The Poisson's ratio was taken as default from [4] and the tensile strength taken as 0.8 times the splitting strength according to [5]. The test results are given in Appendix A and Appendix B and summarised in Table 3-2 and Table 3-3.

Table 3-2 Unconfined static mechanical properties of the concrete material.

Modulus of elasticity [GPa]	Poisson's ratio [-]	Compressive strength [MPa]	Tensile strength [MPa]	Fracture energy [N m^{-1}]
44	0.16	100	5.2	156

Table 3-3 Confined static mechanical properties of the concrete material.

Relative volume ($V_{rel}=V/V_0$) [-]	Volumetric strain $\varepsilon_v=\ln(V_{rel})$ [-]	Pressure $p=-1/3tr(\mathbf{T})$ [MPa]	Unloading and loading bulk modulus $dp/d\varepsilon_v$ [GPa]
1.0000	0.0000	0	9
0.9896	-0.0104	90	9
0.9715	-0.0289	216	-
0.9503	-0.0510	390	-
0.9391	-0.0628	565	-
0.9300	-0.0726	737	25

3.2 Steel material

The steel reinforcement was characterized through uniaxial tension test of a ø12 mm Ks 500 ST rebar. The density and Poisson's ration were set as defaults according to standard tables. The tests were performed at the Swedish National Testing and Research Institute (SP) according to SS-EN 10 002-1 and the results are presented in Table 3-4 and Figure 3-1.

Table 3-4 Static mechanical properties of the reinforcement material.

Mass density [kg m^{-3}]	Modulus of elasticity [GPa]	Poisson's ratio [-]	Yield limit [MPa]	Tensile strength [MPa]
7 800	207	0.3	586	684

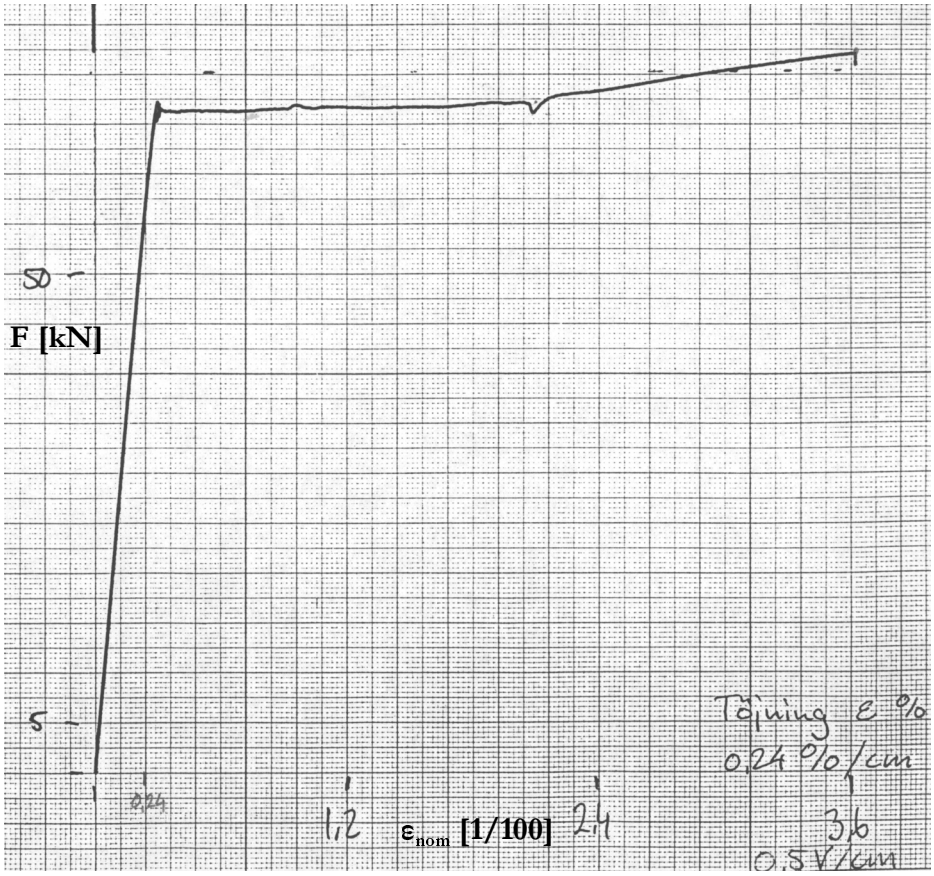

Figure 3-1 Resulting extension curve (Force [kN]-nominal strain [1/100]) from steel rebar material testing.

4 FINITE ELEMENT MODEL

The problem was numerically analysed in the finite element code LS-DYNA version 950d [6]. The computer system used for these simulations is specified in Table 4-1.

Table 4-1 System specifications

Computer	Compaq Workstation XP1000
Processor	667 MHz DEC/Alpha 21264A
Main memory	1 024 MB
Operating system	Digital UNIX version 4.0d
Pre-processor software	LS-INGRID versions 3.5a
Finite element analysis software	LS-DYNA version 950d
Post-processor software	LS-POST version 1.2

4.1 Spatial discretization

Material, or Lagrangian, description of the motion for the whole problem was used. The concrete beam and drop weight were discretized in space with eight-node cube elements. One-point Gauss integration and viscous hourglass control was used for the beam and weight. For the steel-pad and striker-head selectively reduced integration was used. The reinforcement bars were spatially discretized with beam elements and the stirrups with truss elements. For the problem both double and single symmetry were used, see Figure 4-1, and the mesh data is given in Table 4-2.

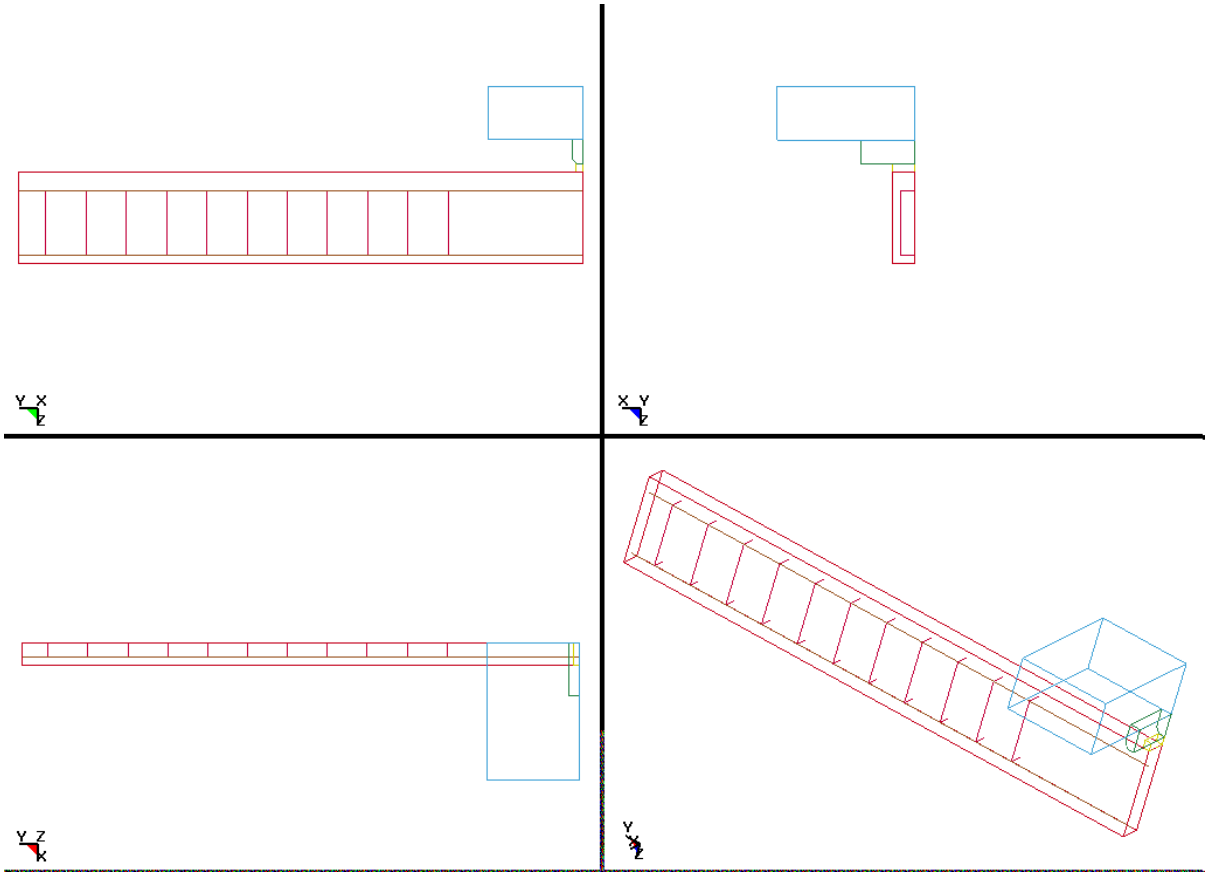

Figure 4-1 Problem geometry

Table 4-2 Mesh size

Nodes	42 871
8-node hexahedron elements	36 823
Truss elements	626
Element sizes	From 10x10x10 mm in the impact zone to 10x10x100 mm at the beam end

4.2 Contact

For the two contact interfaces, striker-steel pad and steel pad-beam, a surface-to-surface constraint algorithm with friction was used. Adjacent beam and reinforcement nodes were merged. The dampers were not incorporated in the model and the problem was only analysed up to 20 ms after impact. Acceleration due to gravity was used for the problem.

5 MECHANICAL CONSTITUTIVE MODELLING

5.1 Concrete material

To model the concrete material the K&C concrete model release III [7] was used. The source code was made available to FOI through an agreement with the developers. Release I of this model is available in the LS-DYNA standard material library as material type 72. The input parameters for the model are valid for one element size only, which results in erroneous fracture energy release when using different element sizes in a problem. Modifications were made to the source code to scale the plastic deformation relative the size of the current element during the unstable cracking, softening phase, of the material. In Figure 5-1 to Figure 5-4 results from simulations of elementary tests with the modified material model using different element sizes are shown together with results with the original model. The response curves displays the same softening behaviour and integration gives the same energy release, i.e. related to fracture energy release the model is independent of the spatial discretization.

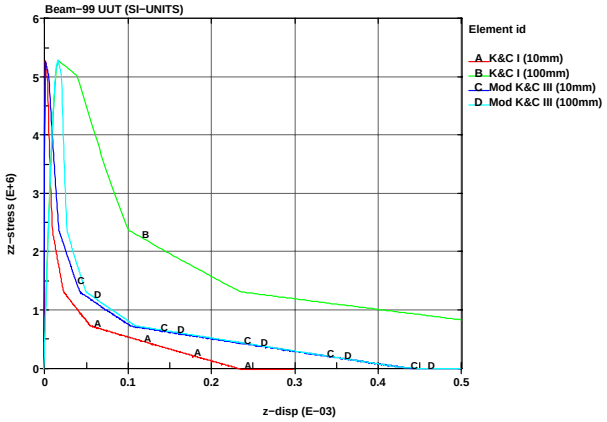

Figure 5-1 Uniaxial extension of single element.

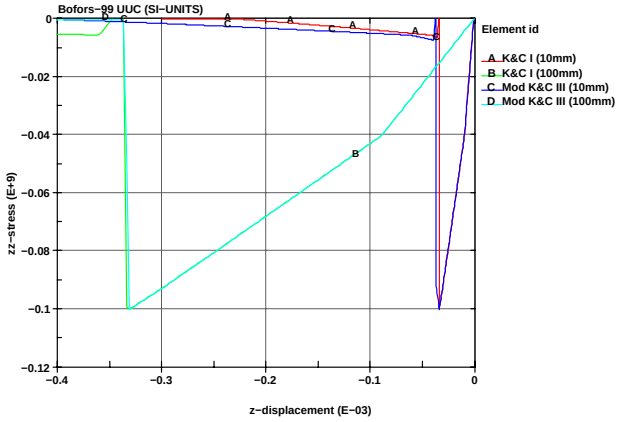

Figure 5-2 Uniaxial compression of single element.

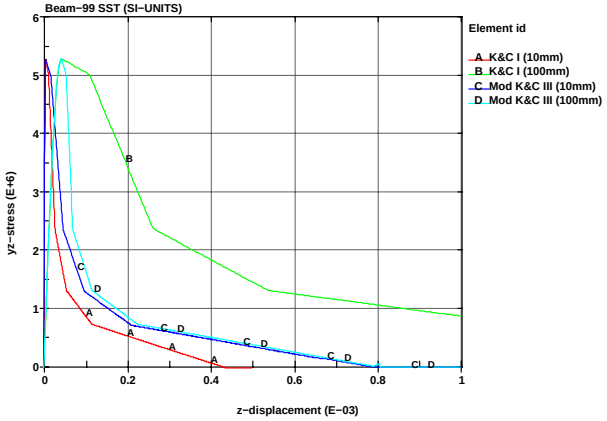

Figure 5-3 Simple shearing of single element.

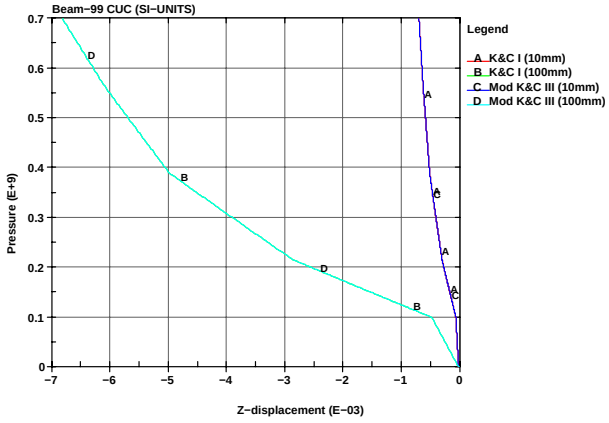

Figure 5-4 Confined uniaxial compression of single element.

In the model, the elastic material properties, except for the Poisson's ratio, are derived from the equation of state. The experimental data on the equation of state in Table 3-3 was complemented with two data points to get a correct elastic wave speed and to get correspondence with the uniaxial data on the modulus of elasticity. The first linear elastic part of the equation of state was constructed using results from uniaxial tension tests. The volumetric strain, pressure and unloading bulk modulus for the first point were calculated as:

$$\begin{cases} \varepsilon_v = \dfrac{0.4 f_{cc}}{E_c}(2\upsilon - 1) = \dfrac{0.4 \cdot 100 \cdot 10^6}{44 \cdot 10^9}(2 \cdot 0.16 - 1) = -0.00062 \\ p = -0.4 \dfrac{1}{3} f_{cc} = -0.4 \cdot \dfrac{1}{3} \cdot 100 \cdot 10^6 = 13.3\ MPa \\ K_u = \dfrac{E_c}{3(1-2\upsilon)} = \dfrac{dp}{d\varepsilon_v} = 21.5\ GPa \end{cases}$$

The second additional point as:

$$\begin{cases} \varepsilon_v = -0.0022 \\ p = -\dfrac{1}{3} f_{cc} = -\dfrac{1}{3} \cdot 100 \cdot 10^6 = 33.3\ MPa \\ K_u = \dfrac{dp}{d\varepsilon_v} = \dfrac{33.3}{0.0022} = 15.2\ GPa \end{cases}$$

These points where then connected to the experimental data in Table 3-3 and the resulting input equation of state together with loading and unloading bulk modulus are shown in Figure 5-5 and Table 5-1.

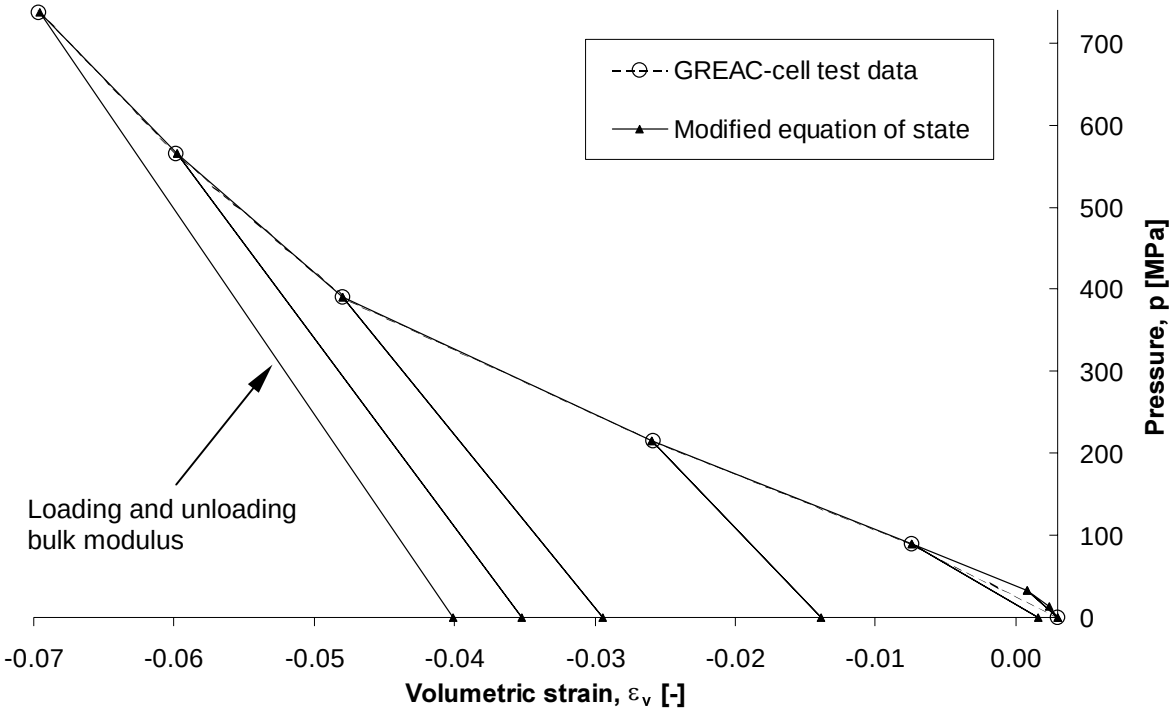

Figure 5-5 Input equation of state with test data from GREAC-test.

Table 5-1 Tabulated equation of state with loading and unloading bulk modulus

Mass density [kg m^{-3}]	Relative volume [-]	Volumetric strain [-]	Pressure [MPa]	Bulk modulus [GPa]
2 390	1.0000	0.0000	0	21.57
2 391	0.9994	-0.0006	13.3	21.57
2 397	0.9978	-0.0022	33.3	15.15
2 415	0.9896	-0.0104	90	10
2 460	0.9715	-0.0289	216	18
2 515	0.9503	-0.0510	390	21
2 545	0.9391	-0.0628	565	23
2 570	0.9300	-0.0726	737	25

The strength surfaces were constructed according to the instructions in [7] and tuned so that the stress path from the unconfined uniaxial compression tests was replicated. Also, the residual strength curve was fitted to the GREAC-test results at high pressures. These strength surfaces are valid only for pressures above one third of the unconfined compressive strength, so the first point on the unconfined compression stress path has no significance. In Figure 5-6 the resulting compression meridians are shown.

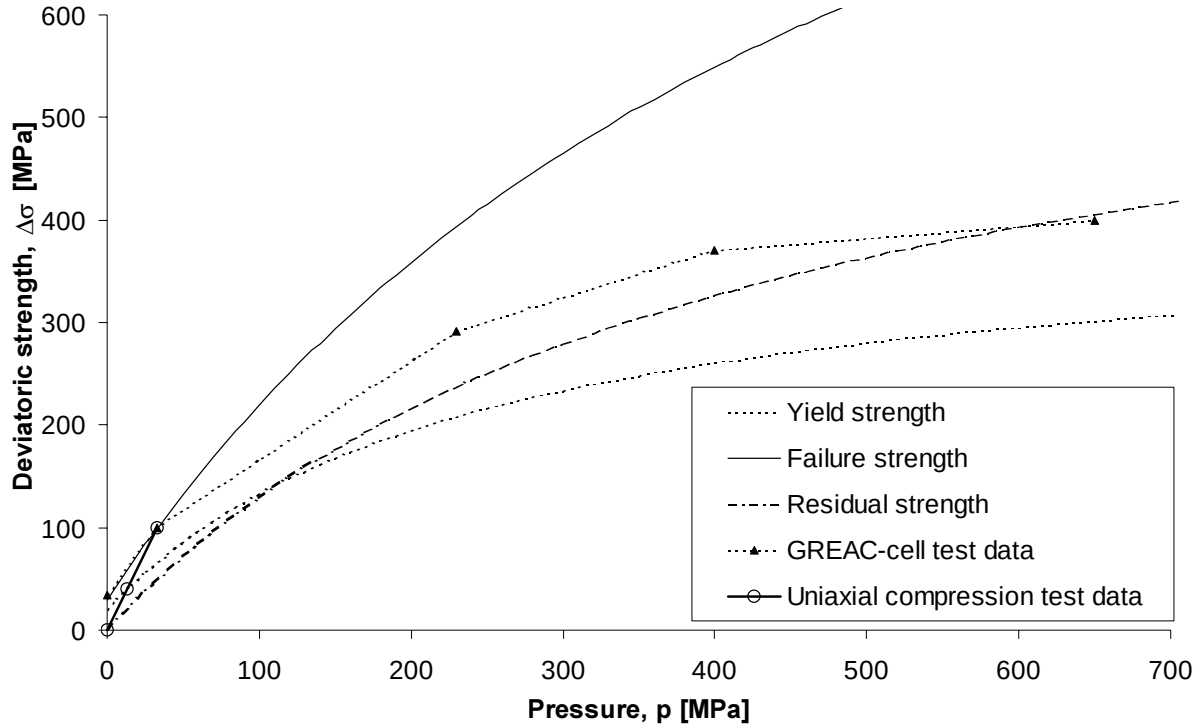

Figure 5-6 Compressive meridians fitted to the unconfined uniaxial and GREAC-cell test data.

To interpolate between these surfaces, i.e. to model the stable and unstable cracking, the model needs the input of a damage function $\eta(\lambda)$ used as

$$\Delta\sigma = \eta(\Delta\sigma_{\max} - \Delta\sigma_{\min}) + \Delta\sigma_{\min}$$

where

$$\Delta\sigma = \sqrt{3J_2}$$

The modified effective plastic strain λ is calculated as

$$\lambda = \begin{cases} \int_0^{\bar{\varepsilon}_p} \dfrac{d\bar{\varepsilon}_p}{r_f\left(1+\dfrac{p}{r_f}f_{ct}\right)^{b1}}, & p \geq 0 \\ \int_0^{\bar{\varepsilon}_p} \dfrac{d\bar{\varepsilon}_p}{r_f\left(1+\dfrac{p}{r_f}f_{ct}\right)^{b2}} + b_3 f_d k_d \left(\varepsilon_v - \varepsilon_v^{yield}\right), & p < 0 \end{cases}$$

where

$$\bar{\varepsilon}_p = \sqrt{\frac{2}{3}\varepsilon_{ij}^p \varepsilon_{ij}^p}$$

$p = -\frac{1}{3}tr(\mathbf{T})$, where $\mathbf{T}$ is the stress tensor

r_f = Strain rate enhancement factor

f_{ct} = Strength in uniaxial extension

k_d = Internal scalar multiplier

$$f_d = \begin{cases} 1 - \dfrac{\left|\sqrt{3J_2}/p\right|}{0.1}, & \left|\sqrt{3J_2}/p\right| < 0.1 \\ 0, & \left|\sqrt{3J_2}/p\right| \geq 0 \end{cases}$$

b_1, b_2, b_3 } Curve fitting parameters

Simulations of uniaxial extension and compression of a single cube element was performed during which the damage function was altered until the right fracture energy release and the maximal crack opening, according to test data and the recommendations in the CEB-FIP model code 90, were obtained. The resulting damage function is given in Figure 5-7 and Table 5-2.

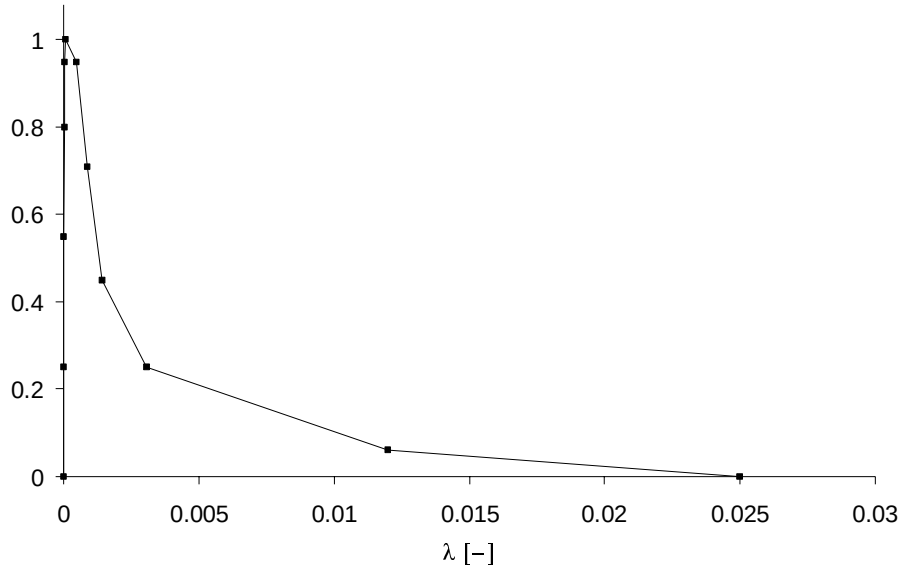

Figure 5-7 Damage function

Table 5-2 Tabulated damage function

λ [–]	0.0	5.5E-6	1.4E-5	2.9E-5	5.1E-5	8.2E-5	4.8E-4	8.6E-4	14.4E-4	30.6E-4	12.0E-3	25.0E-3
η [–]	0.00	0.25	0.55	0.80	0.95	1.00	0.95	0.71	0.45	0.25	0.06	0.00

The material model incorporates the possibility of strength enhancement due to loading rates and for this the bilinear relation given in the CEB-FIP model code 90 [8] was used. Also, it is possible for the user to set the associativity of the flow rule. This is done via a scalar valued parameter with value 0-1, where 0 gives a volume preserving flow rule, i.e. no dilatancy, and 1 implies an associated flow rule.

5.2 Steel material

For the stirrups, a linear elastic-plastic material model with isotropic hardening was used. The material parameters were set according to test data with a hardening modulus of 1 GPa. For the rebars a linear elastic-perfectly plastic material model with the same elastic properties as above was chosen due to restrictions in the code.

5.3 Drop weight material

The drop weight was modelled with a linear elastic material model with a modulus of elasticity of 200 GPa and Poisson's ratio set to 0.3.

6 RESULTS FROM SIMULATIONS AND COMPARISON WITH TEST DATA

The pre-processor input file for the simulation is given in Appendix . The results from the simulations displayed a different behaviour than the test results. In the test cracks in mode I (tension) were initiated, the first approximately 0.3 ms after impact, at the bottom of the beam followed by crushing of the material in the impact zone. The simulations reproduced the first mode I crack but also displayed an almost instantaneous initiation of a mode II (in plane shear) crack 50 mm from the centre point of impact. This crack then propagated through the beam resulting in a partial separation of the material directly under the striker and the rest of the beam. This shear failure allowed for no additional mode I cracks to develop, as well as no crushing of the impact zone. See Figure 6-1 for the damage evolution, i.e. the cracking of the beam.

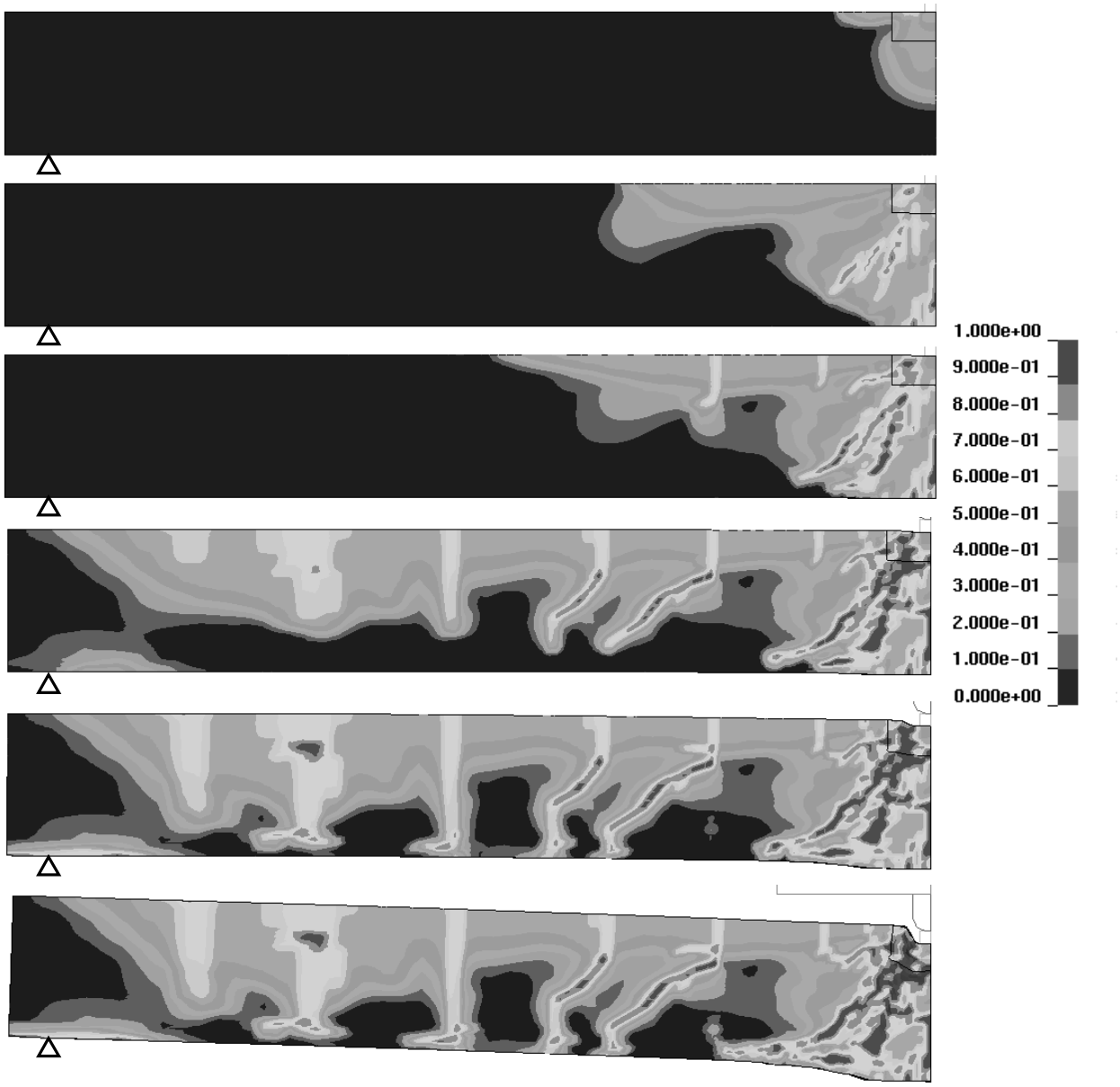

Figure 6-1 Elevation view with fringes of damage variable at times 0.1, 0.3, 0.5, 1, 5 and 20 ms.

Any problems induced by the double symmetry were investigated by performing computations using both single and double symmetry and it was concluded, based on negligible differences in the results, that double symmetry could be used in the problem. As described in chapter 5.1 the associativity of the flow rule can be varied. This was also investigated for the two cases of volume preserving and associative flow rule and it was concluded that this had negligible effect on the results. Three different equations of state were used, see Figure 6-2, but the type of failure changed only slightly.

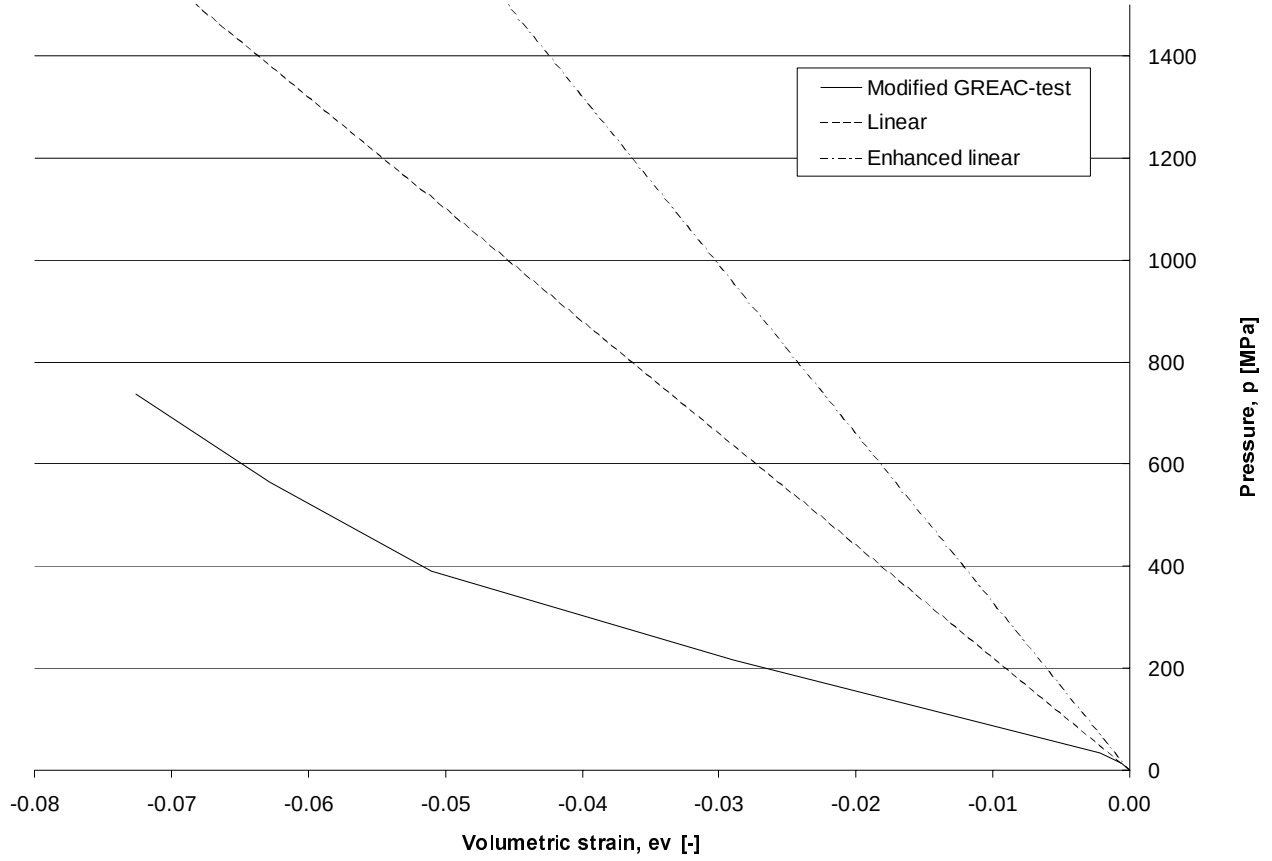

Figure 6-2 The three different equations of state used in the parameter influence analysis.

Comparisons are made below between the registrations from the test and the corresponding data from the numerical analysis. In Figure 6-1 an elevation view with damage plotted on the surface at times 1 and 20 ms respectively.

- **High speed photos**. Comparisons between the high-speed photos and damage plots from the model are given in Figure 6-3 and Figure 6-4.

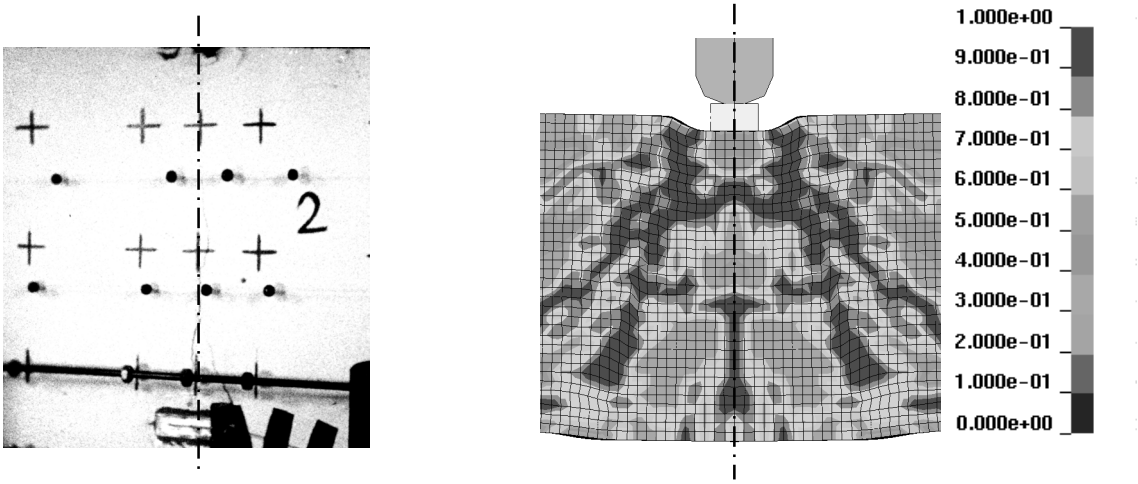

Figure 6-3 High-speed photo at mid-span and numerical damage plot after 0.6 ms. Beam mid-span indicated by dash-dotted line.

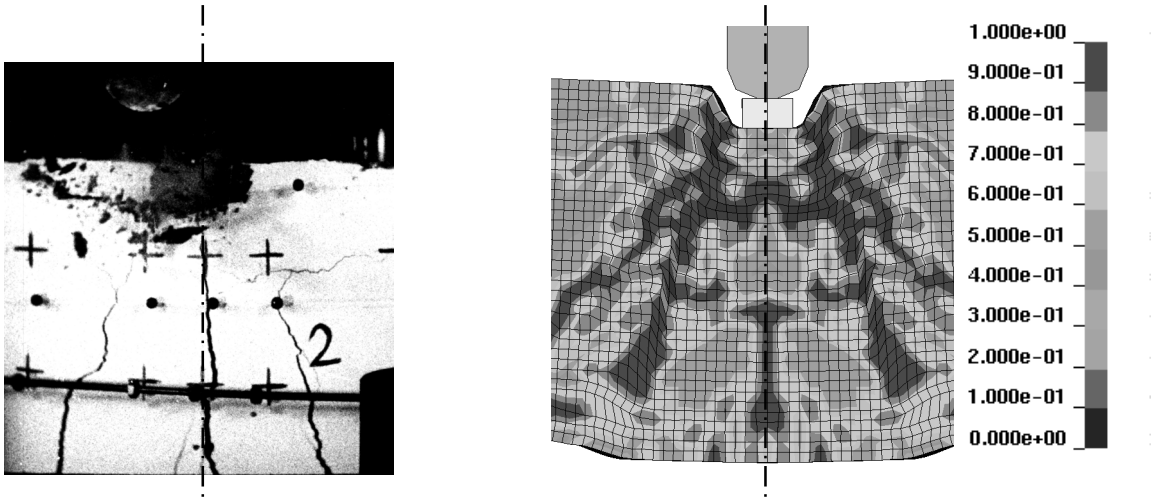

Figure 6-4 High-speed photo at mid-span and numerical damage plot after 20 ms. Beam mid-span indicated by dash-dotted line.

- **Striker displacement**. In the numerical analysis, the striker displacement is greater than in the tests. See Figure 6-5. This is due to the partitioning of the beam caused by the shear failure.

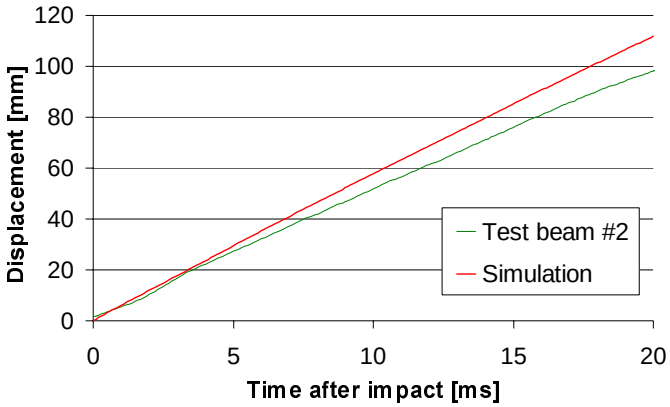

Figure 6-5 Striker displacement (TranS) from test and simulation.

- **Striker head acceleration**. In the test, the peak acceleration is 18000 ms^{-2} and the model gives a rigid body acceleration for the striker head of 8000 ms^{-2}, see Figure 6-6. The lower value from the model can also be explained by the shear-induced failure.

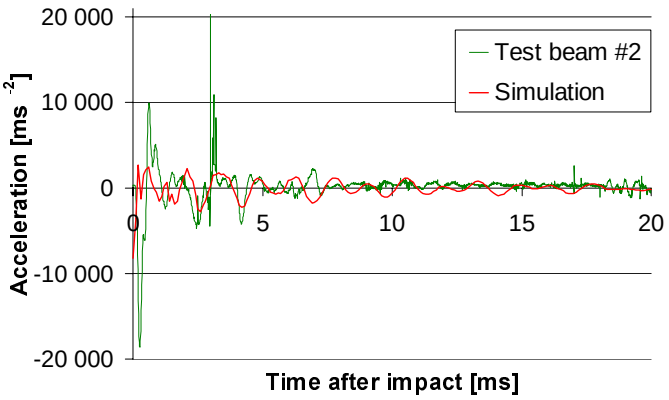

Figure 6-6 Striker head acceleration histories (AccS) from test and simulation.

- **Beam acceleration**. Data on the nodal acceleration was hard to use for comparisons due to oscillations. In Figure 6-7 the acceleration from the simulation was filtered using averaging over nine points. However, integration of the signals shows that the speed of the beam is lower in the model than in test. Again, this is due to the shearing failure.

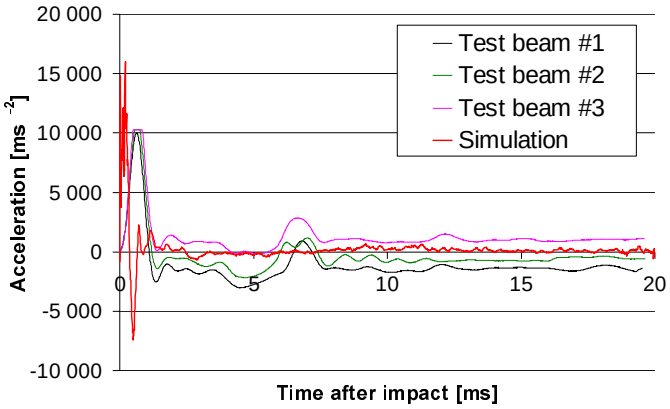

Figure 6-7 Beam acceleration histories (AccL and AccR) from test and simulation.

- **Beam displacement**. The model shows a larger displacement of the mid-centre section of the beam compared to the test, see Figure 6-8. This is in accordance with the striker displacement.

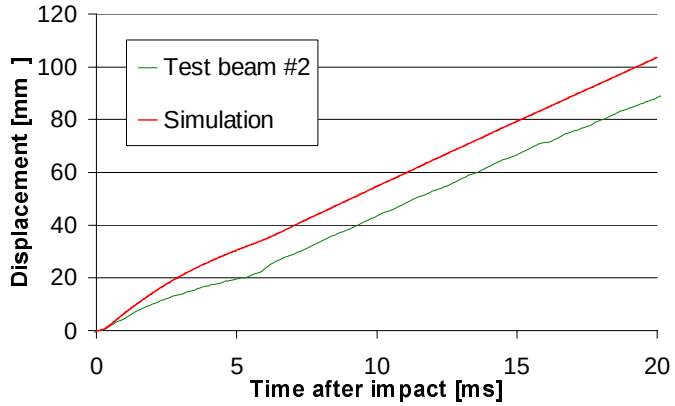

Figure 6-8 Beam mid-section velocity histories (TranB) from test and simulation.

- **Crack indication**. For the mode I crack at the beam's lower surface, the model reproduces well the time for the initiation. A stress-strain plot, see Figure 6-9, reveals that the material behaviour in uniaxial extension is accurately described.

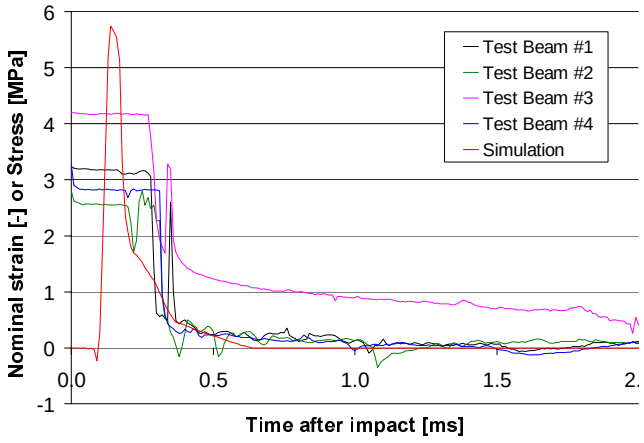

Figure 6-9 Crack indication from test (Crack) and stress history from simulation at beam mid section.

- **Strain in lower rebars (SGR-side).** The strain histories in the model show acceptable agreement with the test in the initial phase, see Figure 6-10.

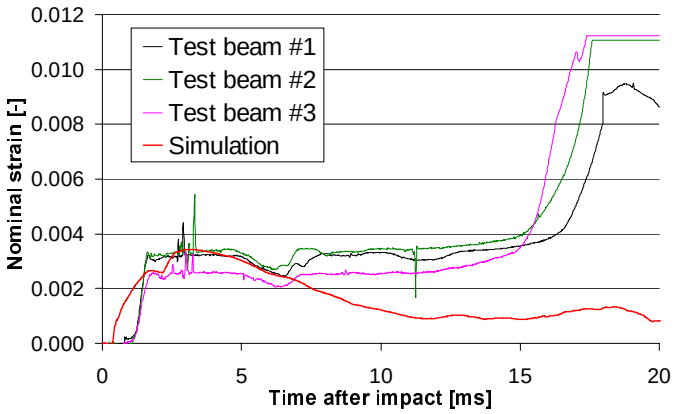

Figure 6-10 Strain histories in lower rebars 200 mm from beam mid section (SGR-mid)

- **Strain in lower rebars (SGR-mid).** The strain histories in the model show good agreement with the test data in the initial phase, see Figure 6-11. The strain gauges reach their maximum range though at approximately one millisecond.

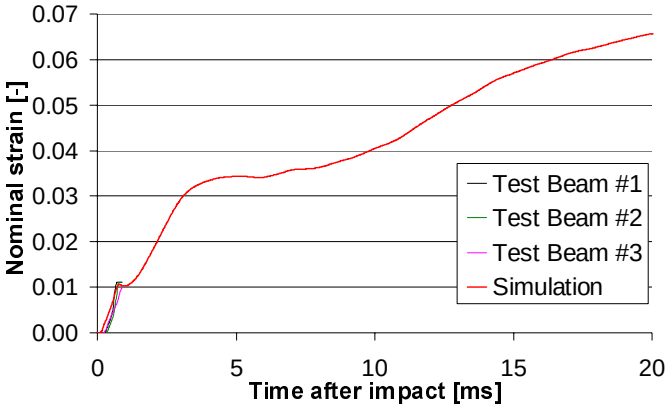

Figure 6-11 Strain histories in lower rebars 200 mm from beam mid section (SGR-mid)

- **Strain in concrete**, at the same height as the tension reinforcement. The strain in the model is slightly smaller than the test data, see Figure 6-12. The strain gauges reaches its maximum range after 0.5 ms.

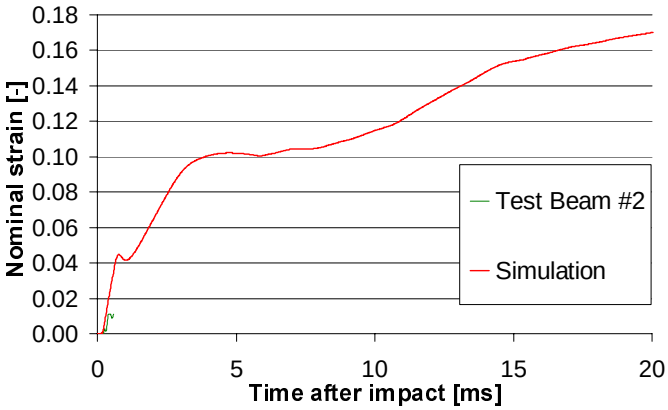

Figure 6-12 Strain histories in concrete at beam mid section (SGC)

7 CONCLUSIONS

An investigation has been carried out to determine if a numerical model could be used to reproduce the results from a drop-weight test on reinforced concrete beams. A short description of the tests performed is given with a reference to the corresponding test data report. Mechanical material characterization was performed on both the concrete and the steel reinforcement material. The data was then adapted to the concrete material model. Simulations were performed to investigate how symmetry, flow rule associativity and the equation of state influenced the results.

The conclusion from this study is that the concrete material model is able to accurately describe material response for standard tests as uniaxial extension and compression. However, it does not seem to be able to reproduce the structural response in the tests performed, given the available data on the material properties and the numerical tool of analysis used. Suggestions for future implementation of the material model are to include:

- The possibility to use full or selectively reduced integration for hexahedral elements. In the current implementation, the model is valid only for one-point integrated hexahedral elements and for the zone near the impact this can be insufficient.
- Inelastic deformations due to isotropic compression, i.e. the volumetric strain from the equation of state, in the model's damage evolution.
- Non-local material behaviour. This is one way to avoid strain localization, as in the present problem, by introducing non-local measures of deformation in the material model [9]. A simple method is to calculate local strains and to choose a domain of influence. A weight function is then applied to the local strains in this domain and the resulting, weighted strain is used to calculate inelastic strain. In the present model inelastic strain is represented by a scalar valued damage parameter.

One way to circumvent problems of localisation is to introduce a non-local strain measure. This way the material failure in a finite element depends on the state of a neighbourhood of the element, see Figure 7-1. In the new LS-DYNA version 960 this has been implemented for solid elements with one-point integration. The strain measure is weighted and integrated over the element neighbourhood using the following expression for the non-local rate of evolution of the modified effective plastic strain λ:

$$\dot{\lambda}(\mathbf{x}_e) = \frac{\sum_{i=1}^{N_r} \dot{\lambda}_{local} w_{ei} V}{\sum_{i=1}^{N_r} w_{ei} V}$$

$$w_{ei} = w(\mathbf{x}_e - \mathbf{x}_i) = \frac{1}{\left[1 + \left(\frac{\|\mathbf{x}_e - \mathbf{x}_i\|}{L}\right)^p\right]^q}$$

where λ_{local} is the local strain measure, w_{ei} is a weight function, $\boldsymbol{x}_e$ is the position vector of the element integration point, $\boldsymbol{x}_i$ is the position vector of a neighbouring element and V_i is the corresponding element volume. L is the radius of the element neighbourhood. Typical values for the weight function parameters p and q are 8 and 2, see Figure 7-2 for the two-dimensional case. In Figure 7-3 and Figure 7-4 these values are used for a parameter analysis for the one-dimensional case.

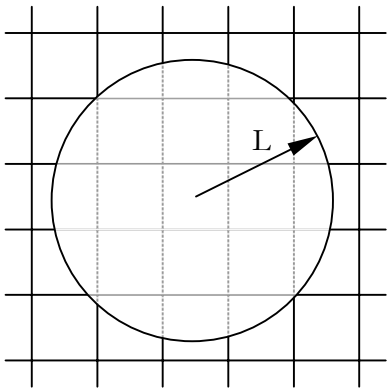

Figure 7-1 Element neighbourhood with radius L.

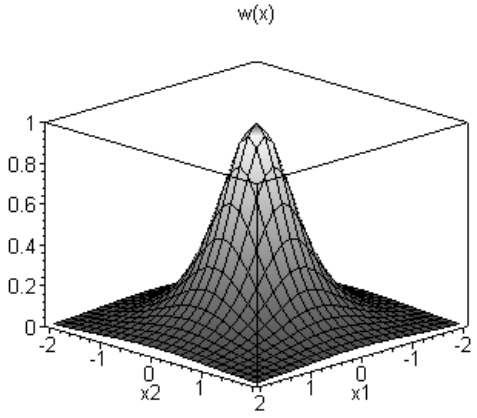

Figure 7-2 Weight function over the element neighbourhood with p=8 and q=2.

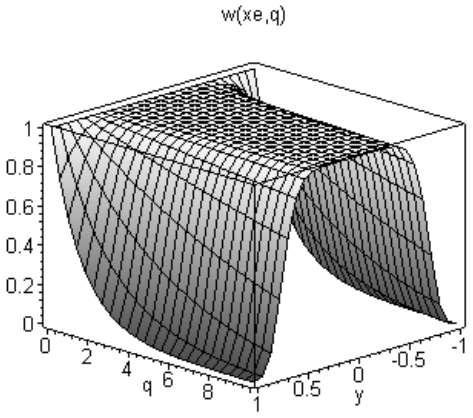

Figure 7-3 Weight function as a function of neighbouring element position and q with p=8.

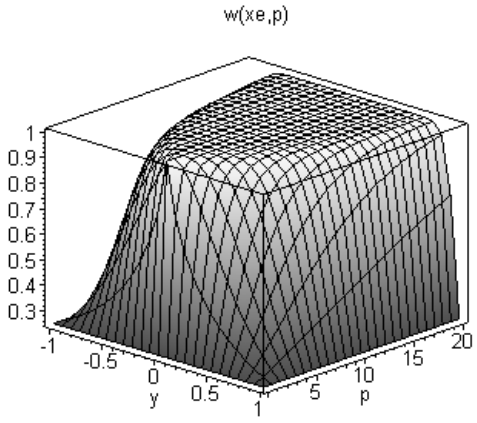

Figure 7-4 Weight function as a function of neighbouring element position and p with q=2.

ACKNOWLEDGEMENTS

The author wishes to thank The Swedish Armed Forces Headquarters who financed this work. Thanks to John E. Crawford, Javier Malvar and Kenneth B. Morrill at Karagozian & Case Structural Engineers (K&C) for supplying the source code and for the discussion on the concrete model. Also, Eric Buzaud at the Centre d'études de Gramat (CEG) on whose opinions and help the author always rely on and appreciate. Finally, thanks to Håkan Hansson and Lars Olovsson at FOI without whom this study would not have been possible to carry out.

REFERENCES

1. Ågårdh, L., J. Magnusson, and H. Hansson, *High strength concrete beams subjected to impact loading - An experimental study*. 1999, Defence research establishment (FOA): Tumba. p. 60.
2. Hilleborg, A., *Determination of the fracture energy of mortar and concrete by means of three-point bend tests on notched beams*. Materials and structures, 1985. **13**: p. 285-290.
3. Ågårdh, L., *Material Test Procedures in Support of Dynamic Material Modelling*. 1999, Defence research establishment (FOA): Tumba. p. 200.
4. *Handbook for concrete, High performance concrete - Material and design (In Swedish)*. 2000, Stockholm: AB Svensk byggtjänst. 419.

5. Ljungkrantz, C., G. Möller, and N. Peterson, eds. *Betonghandbok, Material*. 2 ed. 1994, AB Svensk byggtjänst och Cementa AB: Stockholm. 1127.

6. *LS-DYNA Keyword user's manual, version 950*. 1999, Livermore Software Technology Corporation (LSTC): Livermore. p. 1130.

7. Malvar, L.J., et al., *A plasticity concrete material model for dyna3d*. International Journal of Impact Engineering, 1997. **19**(9-10): p. 847-873.

8. *CEB-FIP model code 1990, Comité euro-international du béton (CEB) et Fédération internationale de la précontrainte (FIP)*. 1993, Thomas Telford: London. 437.

9. Bazant, Z.P. and J. Planas, *Fracture and size effect in concrete and other quasibrittle materials*. 1997, Boca Raton: CRC Press. 616.

RELATED URL:S

www.hkv.mil.se	Swedish Armed Forces Headquarter
www.foi.se	Swedish Defence Research Agency
www.ffi.no	Norwegian Defence Research Institute
www.sp.se	SP Swedish National Testing and Research Institute
www.lstc.com	Livermore Software Technology Corporation
www.kcse.com	Karagozian & Case Structural Engineers
www.optiroc.se	Optiroc AB

APPENDIX A: UNCONFINED STATIC MECHANICAL PROPERTIES OF THE CONCRETE MATERIAL.

Results from elementary material testing on Optiroc performed by FOI. Cubic specimen types had dimensions 150x150mm and the cylindrical types ϕ100x200mm.

Table A-1 Results from concrete testing performed by FOI

Project	Specimen type	Test day	Mass density [kg m^{-2}]	Compressive strength [MPa]	Splitting strength [MPa]	Modulus of elasticity [GPa]	Fracture energy [N m^{-1}]
Slab-97	Cube	72		90.7			
		72		91.1			
		72		72.3			
		72		91.9			
		72			6.2		
		72			5.8		
		72			5.9		
	Rilem[1]	65	2 330	84.2		33.0	154
		65	2 370	87.4		34.8	152
		65	2 360	90.8		37.2	163
Slab-98	Cube	57	2 402	106.2			
		57	2 412	97.5			
		57	2 421	97.1			
		63	2 464		5.9		
		63	2 468		5.2		
		63	2 464		5.6		
	Cylinder	79		100.8		42.8	
		79		99.3		46.6	
		79		99.6		44.1	
Beam-99	Cube	72	2 417	106.5			
		72	2 392	114.8			
		72	2 425	114.3			
		74	2 421		6.5		
		74	2 440		7.2		
		74	2 448		6.4		
		74	2 444		6.6		
	Cylinder	74	2 460	111.5		44.3	
		74	2 445	56.9		42.8	
		74	2 460	96.4		44.2	
Bofors-99	Cylinder[2]		2 390				
			2 390				

[1]: *Sawed cubic and cylindrical (diam70mm) specimens for compressive strength and modulus of elasticity*

[2]: *GREAC-cell test cylinders diam.76x150mm*

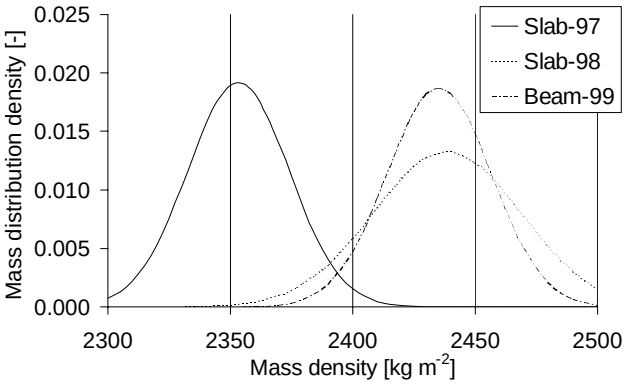

Figure A-1 Mass density frequency function

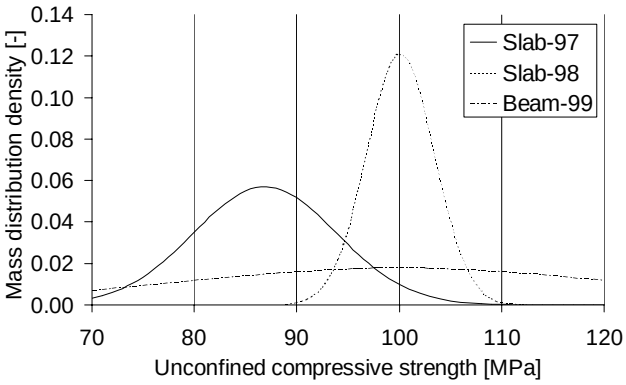

Figure A-2 Uniaxial compressive strength frequency function

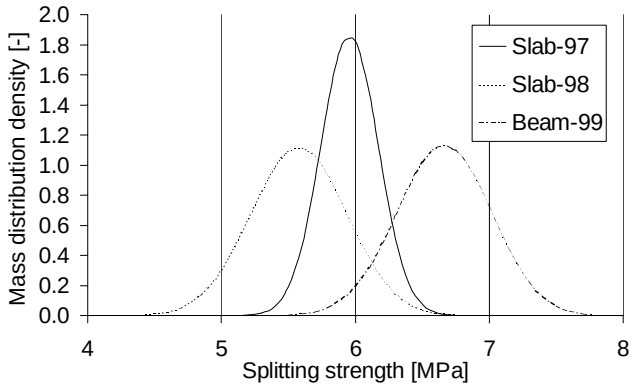

Figure A-3 Splitting strength frequency function.

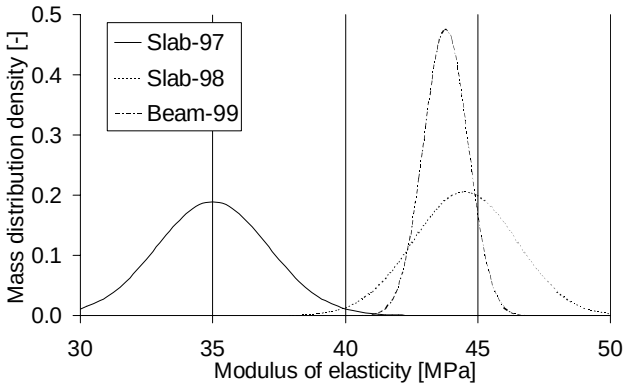

Figure A-4 Modulus of elasticity frequency function

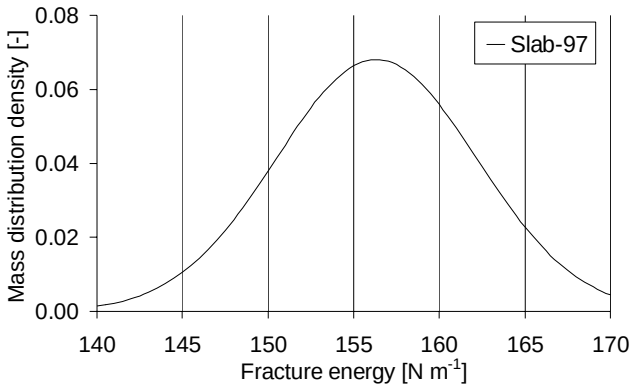

Figure A-5 Fracture energy frequency function

APPENDIX B: CONFINED STATIC MECHANICAL PROPERTIES OF THE CONCRETE MATERIAL.

Results from CREAC-tests on the used concrete material performed by FFI. The following figures show the results from two tests, concrete in thin (Outer diameter O.D.=101.6 mm) and thick (O.D.=122 mm)steel cylinders respectively.

Table B-1 Test specimen data.

Test no	Steel cylinder				Weight of specimen [gram]	Initial length [mm]	Initial density [g/cm^3]	Date of testing
	Outer diameter [mm]	*Inner diameter [mm]*	*Length [mm]*	*Material*				
X	122	76.4	150	Hardened Orvar Supreme	1 624	148.1	2.39	9/11/99
IX	101.6	76.2	150	High strength steel NS 13411-05	1 624	148.7	2.39	15/10/99

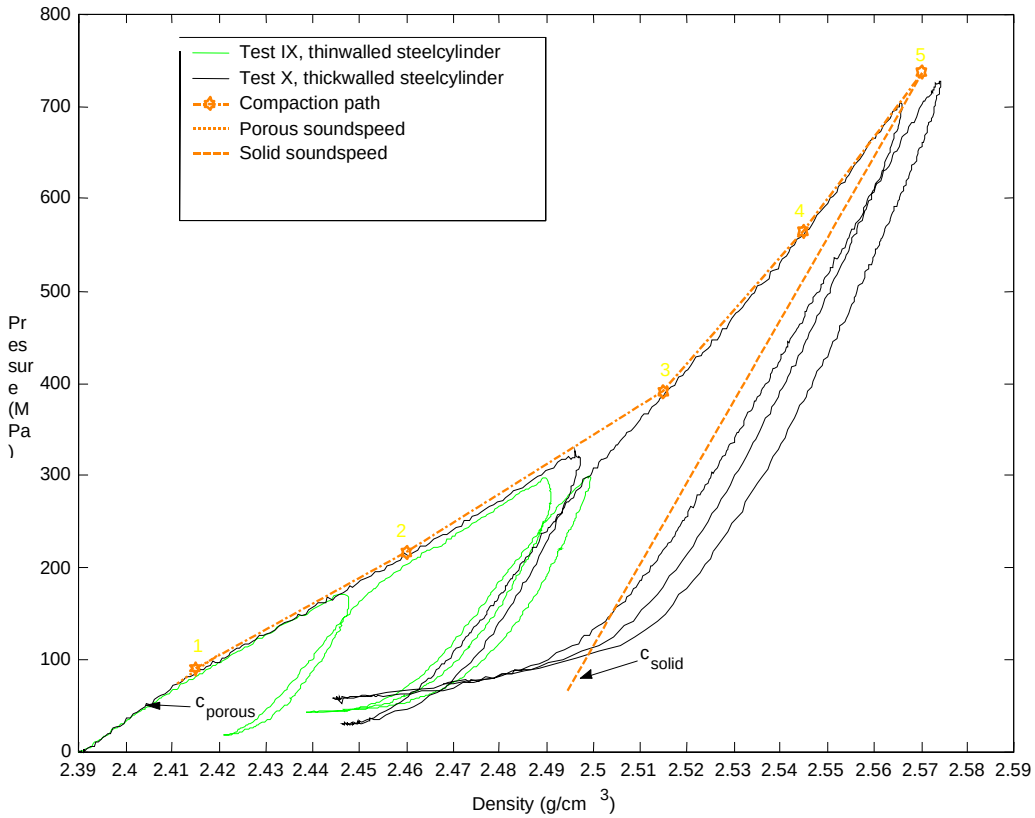

Figure B-1 Pressure versus mass density

Table B-2 Piecewise linear compaction path.

	Mass density [kg m^{-3}]	Relative volume [-]	Volumetric strain [-]	Pressure [MPa]
1	2 390	1.0000	0.0000	0
2	2 415	0.9896	-0.0104	90
3	2 460	0.9715	-0.0289	216
4	2 515	0.9503	-0.0510	390
5	2 545	0.9391	-0.0628	565
6	2 570	0.9300	-0.0726	737

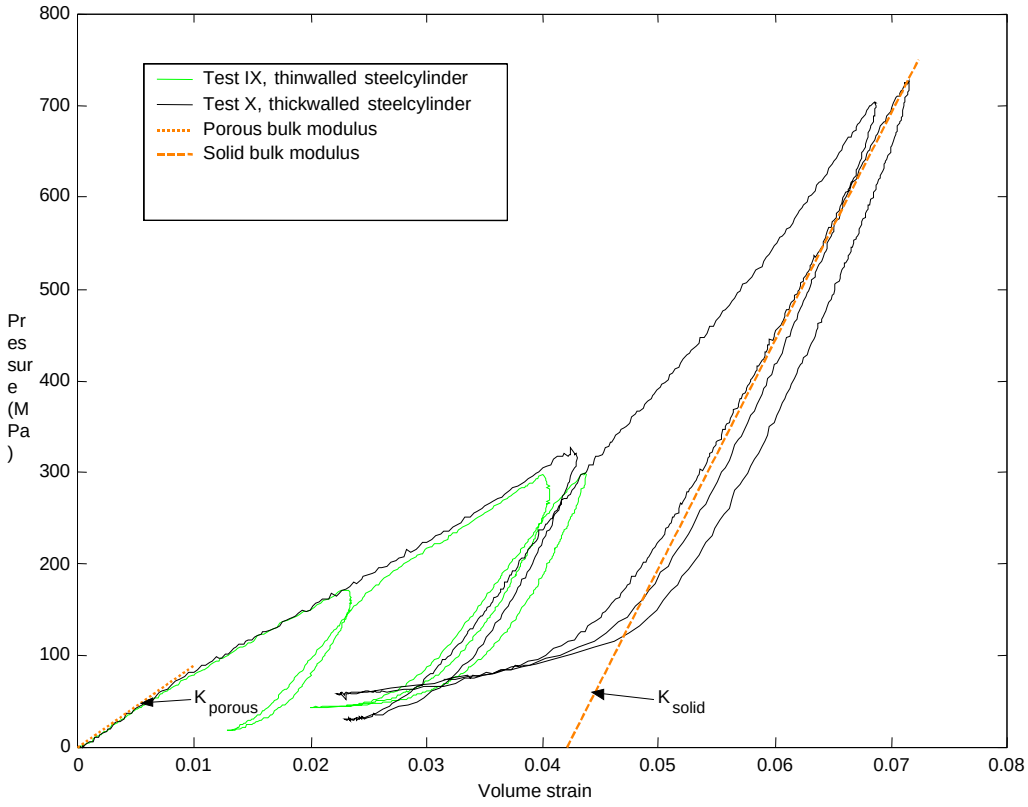

Figure B-2 Pressure versus volumetric strain.

Table B-3 Loading and unloading bulk modulus.

Porous bulk modulus	Solid bulk modulus
$K_p = \frac{p}{\varepsilon_V} = \frac{88}{0{,}01} = 8.8GPa$	$K_p = \frac{p}{\varepsilon_V} = \frac{750}{0{,}072 - 0{,}042} = 25GPa$

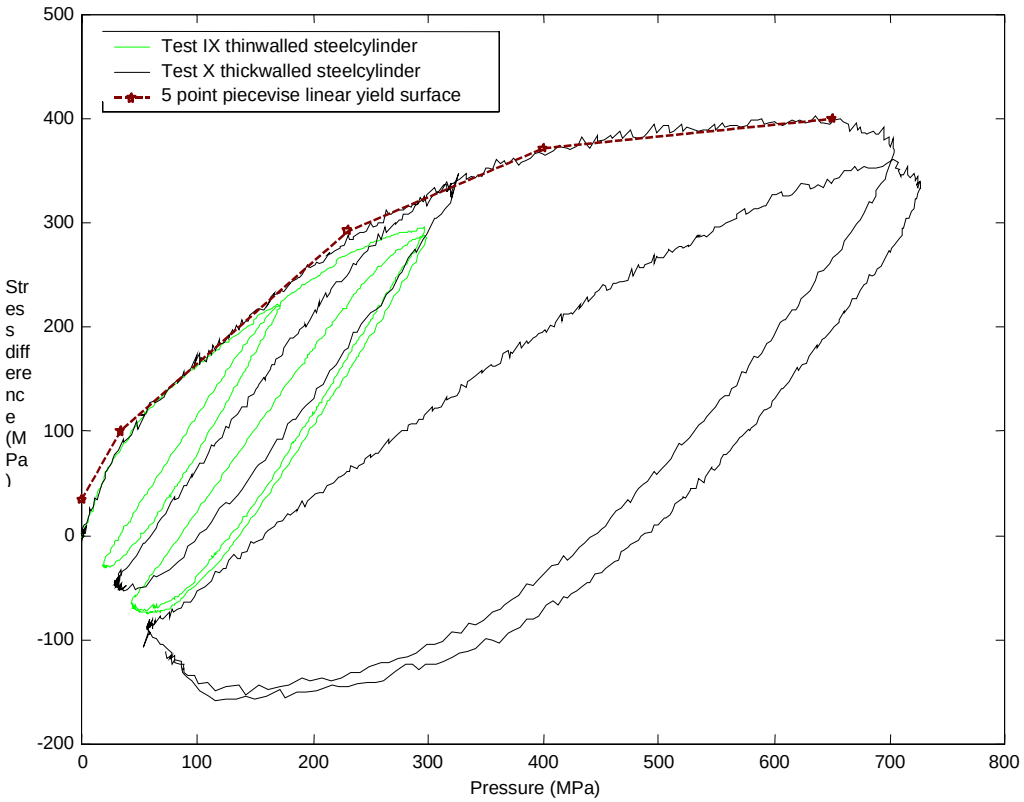

Figure B-3 Stress difference versus pressure.

Table B-4 Five point piecewise linear yield surface.

	Pressure (MPa)	Stress difference (MPa)	Hardening slope
1	0	34	
2	33	100	2,00
3	230	292	0,97
4	400	371	0,46
5	650	400	0,12

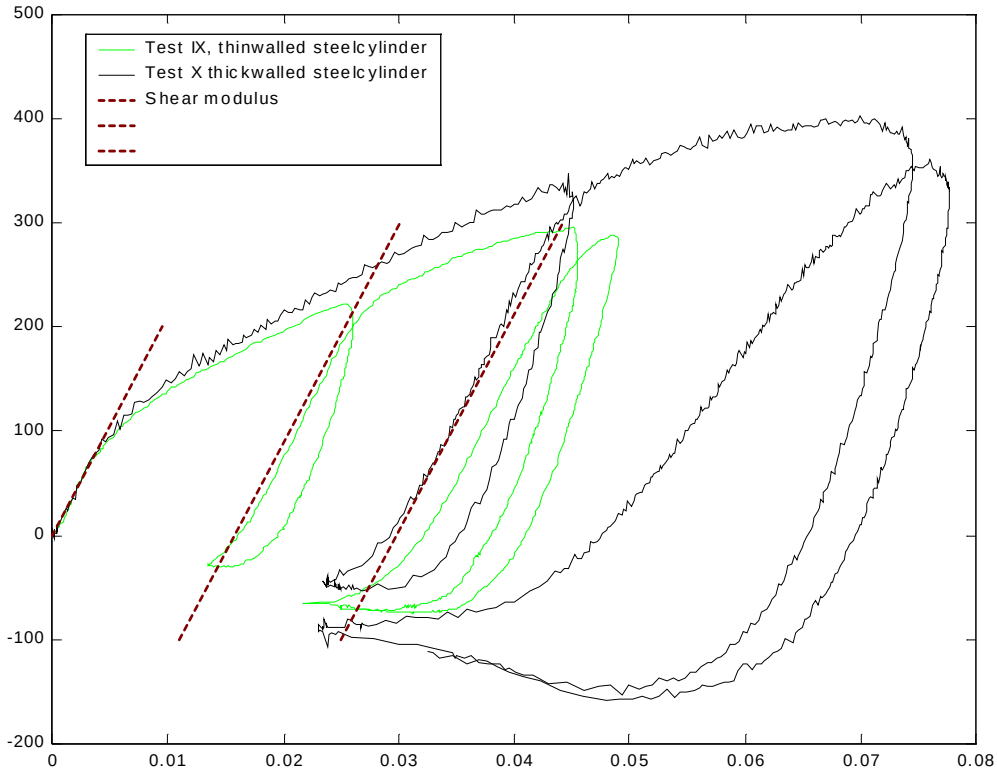

Figure B-4 Stress difference versus strain difference.

Table B-5 Shear modulus.

$G = \frac{1}{2}\frac{ds}{de} = 10.417 GPa$

APPENDIX C: PRE-PROCESSOR INPUT DATA

```
Beam-99 (SI-units)
dn3d kw93
batch
term 20.e-3 plti 1.e-3 tssf 0.25
gmprt elout 0.01e-3 nodout 0.01e-3 glstat 0.1e-3
      rcfo 0.01e-3 nfg 0.01e-3 matsum 0.1e-3;
taurus int8 6;
nfg reaction;
grav 0. 0. -9.8

plane 2
 0. 0. 0. -1.  0.  0. .00001 symm
 0. 0. 0.  0.  1.  0. .00001 symm
sd 1 cyli 0. .01 .06 .01 0. 0. .03
sd 2 plan 0. 0. .09 0. 0. .01
sd 3 plan 0. .04 0. 0. .01 0.
si 1 fric 0.15;
si 2 fric 0.2;
lcd 1 2
c Gravity
 0.0 1.0 1e9 1.0
lcd 2 65
c CEB-FIP model code 90 strength enhancement in tension
3.00E-05 1.000 3.00E-04 1.017 3.00E-03 1.034 3.00E-02 1.051 3.00E-01 1.069
3.00E+00 1.086 3.00E+01 1.105 4.00E+01 1.216 5.00E+01 1.310 6.00E+01 1.392
7.00E+01 1.465 8.00E+01 1.532 9.00E+01 1.593 1.00E+02 1.650 2.00E+02 2.079
3.00E+02 2.380 4.00E+02 2.619 5.00E+02 2.821 6.00E+02 2.998 7.00E+02 3.156
8.00E+02 3.300 9.00E+02 3.432 1.00E+03 3.555 2.00E+03 4.479 3.00E+03 5.127
4.00E+03 5.643 5.00E+03 6.078 6.00E+03 6.459 7.00E+03 6.800 8.00E+03 7.109
9.00E+03 7.394 1.00E+04 7.658 1.10E+04 7.906 1.20E+04 8.138 1.30E+04 8.358
1.40E+04 8.567 1.50E+04 8.767 1.60E+04 8.957 1.70E+04 9.140 1.80E+04 9.316
1.90E+04 9.485 2.00E+04 9.649 3.00E+04 11.045 4.00E+04 12.157 5.00E+04 13.096
6.00E+04 13.916 7.00E+04 14.650 8.00E+04 15.317 9.00E+04 15.930 1.00E+05 16.499
1.10E+05 17.032 1.20E+05 17.533 1.30E+05 18.007 1.40E+05 18.458 1.50E+05 18.887
1.60E+05 19.298 1.70E+05 19.692 1.80E+05 20.071 1.90E+05 20.436 2.00E+05 20.788
2.10E+05 21.129 2.20E+05 21.459 2.30E+05 21.779 2.40E+05 22.091 2.50E+05 22.393

c ************************************************** MATERIAL DEFINITIONS ***
c Concrete dummy material (Material type 72 not avalaible in LS-INGRID)
mat 1
 type 1 ro 2420 e 44.e9 pr 0.16
 brfo 1 hgqt 1
endmat

c Striker weight (density adjusted to fit measured mass)
mat 2
 type 1 ro 4836 e 44.e9 pr 0.16
 brfo 1 hgqt 1
endmat

c Striker head
mat 3
 type 1 ro 7800 e 200.e9 pr 0.3
 brfo 2
endmat

c Striker pad
mat 4
 type 1 ro 7800 e 200.e9 pr 0.3
 brfo 2
endmat
```

```
c Steel rebars
mat 5
 type 28 ro 7800. e 207.e9 pr 0.3 sigy 586.e+6
 beam bform bely care 113.e-6 sare 113.e-6 iss 1.e-9 itt 1.e-9 irr 2.e-9
endmat

c Steel stirrups
mat 6
 type 3 ro 7800. beta 1. e 207.e9 pr 0.3 sigy 586.e6 etan 1.1e9 fs 0.092
 beam bform trus care 79.e-6
endmat

c Concrete dummy material in impact zone (Material type 72 not avalaible in LS-
INGRID)
mat 7
 type 1 ro 2420 e 44.e9 pr 0.16
 brfo 1 hgqt 1
endmat

c ********************************************************** PART DEFINITION ***
c Steel rebars
beam
 rt 000000   0.     0.  0. c mid beam
 rt 000000   0.    .10   0. c accelerometer
 rt 000000   0.    .20   0. c strain gauge
 rt 000000   0.    .50   0. c stirrup
 rt 000000   0.    .65   0. c
 rt 000000   0.    .80   0. c
 rt 000000   0.    .95   0. c
 rt 000000   0.   1.10   0. c
 rt 000000   0.   1.25   0. c
 rt 000000   0.   1.40   0. c
 rt 000000   0.   1.55   0. c
 rt 000000   0.   1.70   0. c
 rt 000000   0.   1.85   0. c stirrup
 rt 000000   0.   2.00   0. c support
 rt 000000   0.   2.10   0. c end
 rt 111111   0.    0.   3. c direction node
0
  1  2 10 5 0 16
  2  3 10 5 0 16
  3  4 30 5 0 16
  4  5 10 5 0 16
  5  6 10 5 0 16
  6  7  9 5 0 16
  7  8  8 5 0 16
  8  9  7 5 0 16
  9 10  6 5 0 16
 10 11  5 5 0 16
 11 12  4 5 0 16
 12 13  3 5 0 16
 13 14  2 5 0 16
 14 15  1 5 0 16
0
 coor 2
  mx 0.055 mz 0.07;
  mx 0.055 mz 0.31;
 lrep 1 2
end

c Steel stirrups
beam
 rt 000000  0.      0.  0.   c n1
```

```
 rt 000000  0.055   0.  0.   c n2
 rt 000000  0.055   0.  0.24 c n3
 rt 000000  0.      0.  0.24 c n4
 rt 111111  1.      0.  0.   c n5 direction node
 rt 111111  0.      0.  1.   c n6 direction node
0
 1 2  6 6 0 6
 2 3 24 6 0 5
 3 4  6 6 0 6
0
 coor 11
  my  0.50 mz 0.07;
  my  0.65 mz 0.07;
  my  0.80 mz 0.07;
  my  0.95 mz 0.07;
  my  1.10 mz 0.07;
  my  1.25 mz 0.07;
  my  1.40 mz 0.07;
  my  1.55 mz 0.07;
  my  1.70 mz 0.07;
  my  1.85 mz 0.07;
  my  2.00 mz 0.07;
 lrep 1 2 3 4 5 6 7 8 9 10 11
end

c Concrete beam
start
 1 7 10;
 1  11  21  51  61  71  80  88
 95 101 106 110 113 115 116;
 1 8 32 35;
c x
  0.000 0.055 0.085
c y
  0.00  0.10  0.20  0.50  0.65  0.80  0.95  1.10
  1.25  1.40  1.55  1.70  1.85  2.00  2.10
c z
  0.00  0.07  0.31  0.34
c Contact surface
 sii+ ; 1 2; -1; 2 m 0. 0. -1.
c Support
 b 0 14 4 0 14 4 001010
 nfg 0 14 4 0 14 4 reaction
c Accelerometer AccL/AccR
 npb 1 2 1;
c Motion history at midspan
 npb 1 1 4;
c Strain gauge SGC
 epb 3 1 3;
 mate 1
c mti ; 1 2; 1 2; 7
end

c Striker weight
start
 1 21 22;
 1 5 6;
 1 2 10;
 0. 0.2 0.515
 0.00 0.04 0.35
 0. .11 .20
 coor 1 mz -.32001; lrep 1;
 velocity 0. 0. 6.7
 mate 2
```

```
end

c Striker head
start
 1 21;
 1 2 3 5;
 1 7 8 10;
 0.00 0.20
 0.00 0.01 0.02 0.02
 0. .06 .07 .07
 di ; 3 4; 3 4;
 sfi ; 2 3; -4; sd 1
 sfi ; -4; 2 3; sd 1
 sfi ; 1 2; -4; sd 2
 sfi ; -4; 1 2; sd 3
 coor 1 mz -.12001; lrep 1;
 velocity 0. 0. 6.7
 sii- ; 1 3; -4; 1 s 0. 0. -1.
 mate 3
end

c Striker pad
start
 1 9;
 1 3;
 1 4;
 0.  .085
 0. .025
 0. .03
 coor 1 mz -.03; lrep 1;
 sii+ ;; -1; 1 m 0. 0. -1.
 sii- ;; -2; 2 s 0. 0. -1.
 mate 4
end

c ******************************************************** LS-INGRID COMMANDS ***
end
tp 0.0001
continue

c ************************************************** CHANGES IN KEYWORD FILE***

*MAT_CONCRETE_DAMAGE
         1      2420      0.16
     5.3E6    29.6E6     .4463  8.08E-10
    19.3E6     0.625   2.58E-9     0.625    1.5E-9       1.6      1.35      1.15
                                                            2
$ 10mm
    5.5E-6    1.4E-5    2.9E-5    5.1E-5    8.2E-5   4.80E-4  8.600E-4  14.40E-4
 30.600E-4    12.E-3    25.E-3   11.E+11
       .25       .55        .8       .95        1.       .95       .71       .45
       .25       .06        .0        .0
*EOS_TABULATED_COMPACTION
         1 0.0000000 0.0000000 1.0000000
     0.00000E+00    -6.00000E-04    -2.20000E-03    -1.04000E-02    -2.89000E-02
    -5.10000E-02    -6.28000E-02    -7.26000E-02     0.00000E+00     0.00000E+00
     0.00000E+00     1.33333E+07     3.33333E+07     9.00000E+07     2.16000E+08
     3.90000E+08     5.65000E+08     7.37000E+08     0.00000E+00     0.00000E+00
     0.00000E+00     0.00000E+00     0.00000E+00     0.00000E+00     0.00000E+00
     0.00000E+00     0.00000E+00     0.00000E+00     0.00000E+00     0.00000E+00
     2.16000E+10     2.16000E+10     1.52000E+10     1.00000E+10     1.80000E+10
     2.10000E+10     2.30000E+10     2.50000E+10     0.00000E+00     0.00000E+00
```

Issuing organization	Report number, ISRN	Report type
FOI – Swedish Defence Research Agency Weapons and Protection SE-147 25 Tumba	FOI-R--0167--SE	User report
	Research area code 5. Combat	
	Month year October 2001	**Project no.** E2011
	Customers code 5. Contracted Research	
	Sub area code 53 Protection and Fortification Techniques	
Author/s (editor/s) Mattias Unosson	**Project manager** Håkan Hansson	
	Approved by	
	Scientifically and technically responsible	

Report title

Modelling of concrete material behaviour with application to reinforced concrete beams subjected to impact.

Abstract (not more than 200 words)

This report presents a finite element analysis of impact loading tests for reinforced concrete beams. The purpose of the work was to evaluate the ability of the chosen numerical method and material models to predict the material and structural response. The impact loading was carried out using a drop weight impacting a simply supported beam at mid-span. Four beams, reinforced with steel rebars and stirrups, were tested. The velocity of the drop-weight and the beam, the strain history of lower reinforcement bars and the acceleration history of the beam were registered and a high-speed film camera captured the crack development. The finite element analysis gave a different type of failure compared to the tests. In the test, the failure was mode I cracking combined with crushing in the impact zone, whereas in the simulations, the failure was mainly due to mode II cracking. Changes were made to the model and to the material data but the results from the test could not be reproduced. The conclusion is that the chosen concrete material model does not seem to be capable of correctly describing the problem, given the material properties and the numerical tool of analysis.

Keywords

impact loading, high performance concrete, finite element analysis, material model, material characterization

Further bibliographic information	Language English
ISSN 1650-1942	**Pages** 34 p.
	Price acc. to pricelist
	Security classification Unclassified

Utgivare	Rapportnummer, ISRN	Klassificering
Totalförsvarets Forskningsinstitut - FOI Vapen och skydd 147 25 Tumba	FOI-R--0167--SE	Användarrapport
	Forskningsområde 5. Bekämpning	
	Månad, år Oktober 2001	**Projektnummer** E2011
	Verksamhetsgren 5. Uppdragsfinansierad verksamhet	
	Delområde 53 Skydd och anläggningsteknik	
Författare/redaktör Mattias Unosson	**Projektledare** Håkan Hansson	
	Godkänd av	
	Tekniskt och/eller vetenskapligt ansvarig	

Rapportens titel (i översättning)

Modellering av betongmaterialbeteende med tillämpning på stötbelastade armerade betongbalkar.

Sammanfattning (högst 200 ord)

I denna rapport presenteras en finit elementanalys av stötbelastning av betong balkar med konventionell armering. Syftet med detta arbete var att utvärdera möjligheten att med valt analysverktyg och materialmodell kunna förutsäga material och strukturresponsen. Stötbelastningen utfördes med en fallvikt som slog an den enkelt upplagda balken i dess mittspann. Totalt genomfördes fyra fallviktsförsök. Under försöken registrerades fallviktshastighet, balkhastighet, balkacceleration, töjning i de nedre armeringsstängerna och på betongytan. En höghastighetskamera fångade skadeprocessen. Finita elementanalysen gav en annan typ av brott än den i försöken. Vid försöken skedde brottet genom sprickpropagering i främst mod I kombinerat med krossning i anslagszonen och i simuleringen skedde brottet främst pga sprickor i mod II. Förändringar gjordes i modellen och i materialdata men, resultatet från försöken kunde inte återskapas. Slutsatsen är att materialmodellen inte kan beskriva problemet på ett korrekt sätt, givet det här använda analysverktyget och materialdata.

Nyckelord

stötbelastning, högpresterande betong, finit elementanalys, materialmodell, materialkarakterisering

Övriga bibliografiska uppgifter	**Språk** Engelska
ISSN 1650-1942	**Antal sidor:** 34 s.
Distribution enligt missiv	**Pris: Enligt prislista** **Sekretess** Öppen